

GENERIC GRAVITATIONAL WAVE SIGNALS FROM THE COLLAPSE OF ROTATING STELLAR CORES

H. DIMMELMEIER

*Department of Physics, Aristotle University of Thessaloniki,
GR-54124 Thessaloniki, Greece*

C. D. OTT

*Department of Astronomy and Steward Observatory, University of Arizona,
Tucson, AZ 85721, U.S.A.*

H.-T. JANKA, A. MAREK, E. MÜLLER

*Max Planck Institute for Astrophysics, Karl-Schwarzschild-Str. 1,
D-85741 Garching, Germany*

We present detailed results from performing general relativistic (GR) simulations of stellar core collapse to a proto-neutron star, using a microphysical equation of state (EoS) as well as an approximate description of deleptonization during the collapse phase. We show that for a wide variety of rotation rates and profiles the gravitational wave (GW) burst signals from the core bounce are of a generic type, already known as Type I in the literature. In addition, for most models the characteristic frequency of the GW burst signal lies in a narrow range around approximately 718 Hz. In our systematic study, using both GR and Newtonian gravity, we identify, individually quantify, and discuss in detail the micro- and macrophysical mechanisms leading to this result, i.e. the effects of rotation, the EoS, and deleptonization. We also discuss the detectability prospects of such GW burst signals by GW detectors, and infer that such a generic type of signal templates will likely facilitate a more efficient search in current and future detectors of both interferometric and resonant type.

1 Introduction

Theoretical predictions of the gravitational wave (GW) signal produced by the collapse of a rotating stellar iron core to a proto-neutron star (PNS) in a core collapse supernova are complicated, as the emission mechanisms are very diverse. While the prospective GW burst signal from the collapse, bounce, and early postbounce phase is present only when the core rotates^{1,2,3,4,5,6,7}, GW signals with sizeable amplitudes can also be expected from convective motions at later post-bounce phases, anisotropic neutrino emission, excitation of various oscillations in the PNS, or nonaxisymmetric rotational instabilities^{9,10,11,12,7,13}.

In the observational search for GWs from merging binary black holes or neutron stars, powerful data analysis algorithms like matched filtering are applied, as the waveform from the inspiral phase can be modeled very accurately¹⁴. In stark contrast, the GW burst signal from stellar core collapse and bounce cannot yet be predicted with the desired accuracy and robustness. First, a general relativistic (GR) description of consistently coupled gravity and hydrodynamics including the important microphysics is necessary. Only very few multi-dimensional codes have

recently begun to approach these requirements. Second, the rotation rate and profile of the progenitor core are not very strongly constrained by either observation or numerical modeling of stellar evolution. Therefore, the influence of rotation on the collapse dynamics and thus the GW burst signal must be investigated by computationally expensive parameter studies.

Previous simulations, considering a large variety of rotation rates and profiles in the progenitor core but ignoring complex (though essential) microphysics and/or the influence of GR, found qualitatively and quantitatively different types of GW burst signals (see, e.g., the work by ^{2,3,4}). These can be classified depending on the collapse dynamics: *Type I* signals are emitted when the collapse of the homologously contracting inner core is not strongly influenced by rotation, but stopped by a *pressure-dominated bounce* due to the stiffening of the EoS at nuclear density ρ_{nuc} where the adiabatic index γ_{eos} rises above 4/3. This leads to an instantaneous formation of the PNS with a maximum core density $\rho_{\text{max}} \geq \rho_{\text{nuc}}$. *Type II* signals occur when centrifugal forces, which grow during contraction due to angular momentum conservation, are sufficiently strong to halt the collapse, resulting in consecutive (typically multiple) *centrifugal bounces* with intermediate coherent re-expansion of the inner core, seen as density drops by often more than an order of magnitude; thus here $\rho_{\text{max}} < \rho_{\text{nuc}}$ after bounce. *Type III* signals appear in a pressure-dominated bounce when the inner core has a very small mass at bounce due to a soft subnuclear EoS or very efficient electron capture.

In contrast, new GR simulations of rotational core collapse employing a microphysical EoS and an approximation for deleptonization during collapse ^{7,8} show that the GW burst signature is exclusively of Type I. In a recent study, we considerably extended the number of models and comprehensively explored a wide parameter space of initial rotation states ⁸. Also for this more general setup we found GW signals solely of Type I form. We identified the physical conditions that lead to the emergence of this generic GW signal type and quantified their relative influence. These results strongly suggest that the waveform of the GW *burst* signal from the collapse of rotating iron cores in a supernova event is much more generic than previously thought. In this work we recapitulate the results presented in ⁸ and discuss the mechanisms which lead to uniformity of the signal type in rotational supernova core collapse to a PNS in more detail.

2 Model Setup and Numerical Methods

We perform all simulations in 2 + 1 GR using the CoCoNuT code ^{4,15}, approximating GR by the conformal flatness condition (CFC) ^{16,17}, whose excellent quality in the context of rotational stellar core collapse has been demonstrated extensively (see, e.g., the result presented in ^{18,7}). CoCoNuT utilizes spherical coordinates with the grid setup specified in ⁷ and assumes axisymmetry. GR hydrodynamics is implemented via finite-volume methods, piecewise parabolic reconstruction, and an approximate Riemann solver. We use Eulerian spherical coordinates and assume axisymmetry for the core-collapse simulations discussed here. The computational grids consist of 250 logarithmically-spaced and centrally-condensed radial zones with a central resolution of 250 m and 45 equidistant angular zones covering 90°. GWs are extracted using a variant of the Newtonian quadrupole formula (see, e.g., the definition in ¹⁸).

We employ the microphysical EoS of Shen et al. ¹⁹ in the implementation of Marek et al. ²⁰. Deleptonization by electron capture onto nuclei and free protons is proposed by Liebendörfer ²¹: During collapse the electron fraction Y_e is parameterized as a function of density based on data from neutrino radiation-hydrodynamic simulations in spherical symmetry ²⁰ using the latest available electron capture rates ²² (updating recent results ⁷ where standard capture rates were used). After core bounce, Y_e is only passively advected and further lepton loss is neglected. Again following the formalism in ²¹, above the trapping density at $\rho_{\text{trap}} = 2.0 \times 10^{12} \text{ g cm}^{-3}$ contributions due to neutrino radiation pressure P_ν are taken into account.

As initial data we take the non-rotating 20 M_\odot solar-metallicity progenitor s20.0 from ²³,

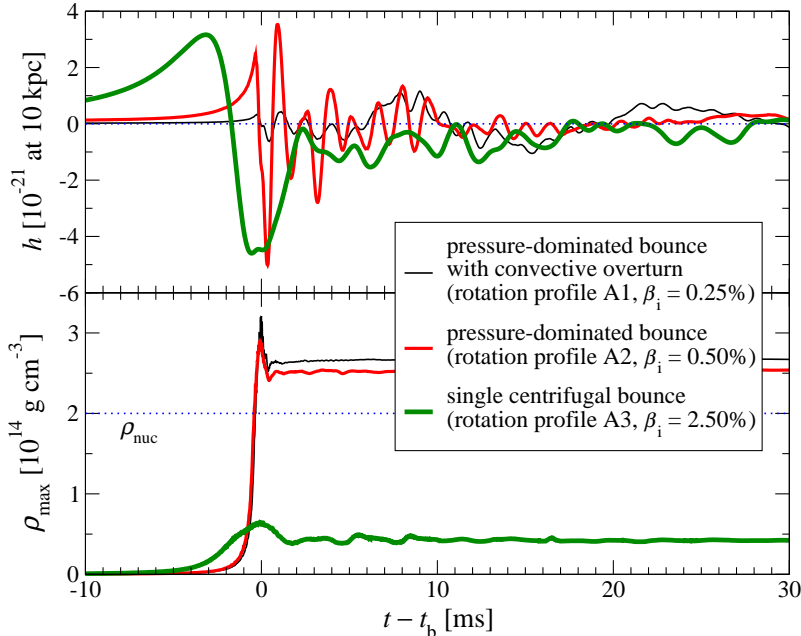


Figure 1: Time evolution of the GW amplitude h and maximum density ρ_{\max} for three representative models with different rotation profiles and initial rotation rates β_i . The model with slow and almost uniform initial rotation (black curve) develops considerable prompt post-bounce convection visible as a lower-frequency contribution in the waveform, while waveform for the model with moderate rotation (red curve) exhibits a regular ring-down. The maximum density of the rapidly rotating model which undergoes centrifugal bounce (green curve) remains always below nuclear density ρ_{nuc} . Time is normalized to the time of bounce t_b .

imposing the rotation law discussed in ^{6,4}. In order to determine the influence of different angular momentum on the collapse dynamics, we parameterize the initial rotation of our models in terms of the differential rotation parameter A (A1: $A = 50,000$ km, almost uniform; A2: $A = 1,000$ km, moderately differential; A3: $A = 500$ km, strongly differential) and the initial rotation rate $\beta_i = T/|W|$, which is the ratio of rotational energy to gravitational energy (approximately logarithmically spaced in 18 steps from 0.05% to 4%).

3 Results

3.1 Generic Type of the Collapse and the Gravitational Wave Signal

As already conjectured in ⁷ and confirmed in ⁸, in the entire investigated parameter space our models yield GW burst signals of Type I, i.e. the waveform exhibits a positive pre-bounce rise and then a large negative peak, followed by a ring-down (upper panel of Fig. 1). However, with respect to collapse dynamics and the relevant forces halting the collapse, the models fall into two classes. While for instance all models with the almost uniform rotation profile A1 experience a pressure-dominated bounce for which a Type I waveform is expected, models with profiles A2 or A3 *and* sufficiently high initial rotation rate β_i ($\geq 4\%$ for A2; $\geq 1.8\%$ for A3) show a *single* centrifugal bounce at subnuclear density (lower panel of Fig. 1). Nevertheless, they also produce a Type I waveform, as their core does not re-expand after bounce to densities much less than those reached at bounce but immediately settles to a PNS after a short ring-down phase. What obviously distinguishes models with pressure-dominated bounce from those with centrifugal bounce is that the latter have GW signals with significantly lower average frequencies. Note also that models with very little rotation develop convective overturn of the shock-heated layer immediately after shock stagnation (not to be confused with the late-time convection discussed in ¹⁰), resulting in a lower-frequency contribution to the post-bounce GW signal (see Fig 1). These long-lasting, almost undamped convective motions are an artifact of our insufficient neutrino treatment *after* the core bounce and are efficiently suppressed if a more accurate description for neutrinos like Boltzmann transport is utilized ¹⁰.

In order to analyze the absence of Type II signals, in particular for cases with centrifugal bounce, we now separately investigate and quantify the influence of GR, a microphysical EoS,

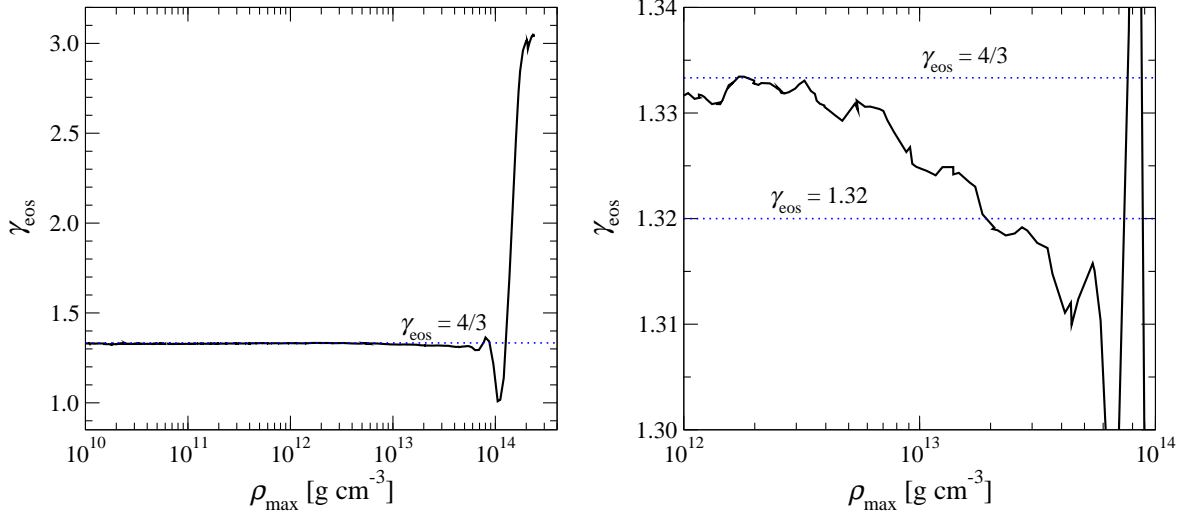


Figure 2: Left panel: Adiabatic index γ_{eos} of the microphysical EoS in the entire density range of the maximum density ρ_{max} in the core during the collapse of a nonrotating model. Although ρ_{max} , which is obtained in the center of the core, does not follow a trajectory of constant entropy, s is still approximately conserved in the pre-bounce phase. Right panel: Magnified view of γ_{eos} in the dynamically most relevant density range between 10^{12} and 10^{14} g cm^{-3} . The average value of γ_{eos} in this density regime is approximately 1.32.

and deleptonization on the dynamics of rotational core collapse with different amounts and distributions of angular momentum. When the pre-collapse iron core starts to contract, its *effective* adiabatic index γ_{eff} is lower than the critical value $\simeq 4/3$ needed for stability against gravitational collapse. Here γ_{eff} is the sum of the adiabatic index $\gamma_{\text{eos}} = \partial \ln P / \partial \ln \rho|_{Y_e, s}$ of the EoS (where P is the pressure, ρ the density, and s the specific entropy of the fluid) and a possible correction due to deleptonization (which can be significant until neutrino trapping sets in at ρ_{trap} ; see ²). At this stage, both GR and rotational effects (in our range of β_i) are negligible in discussing stability. If the build-up of centrifugal forces in the increasingly faster spinning core during collapse is strong enough, contraction is halted and the core undergoes a centrifugal bounce rather than reaching nuclear density (where the stiffening of the EoS with $\gamma_{\text{eos}} \gtrsim 2 \gg 4/3$ would also stop the collapse; see left panel of Fig. 2).

3.2 Influence of General Relativistic Gravity

A necessary condition for a centrifugal bounce at subnuclear densities is that γ_{eff} exceeds a critical rotation index γ_{rot} . There exists a simple Newtonian analytic relation ²⁴, $\gamma_{\text{rot}} = (4 - 10\beta_{\text{ic,b}})/(3 - 6\beta_{\text{ic,b}})$ (where $\beta_{\text{ic,b}}$ is the inner core's rotation rate at bounce), which works well in equilibrium, but is rather imprecise as a criterion for centrifugal bounce in a dynamical situation. For instance, for rotating core collapse models in Newtonian gravity with a simple hybrid EoS ²⁵ and no deleptonization (where $\gamma_{\text{eff}} = \gamma_{\text{eos}}$), we find that for our range of initial rotation rates and $1.24 \leq \gamma_{\text{eff}} \leq 1.332$, the analytic relation strongly underestimates the actual γ_{rot} by up to ~ 0.2 at high $\beta_{\text{ic,b}}$, as shown in Fig. 3. Furthermore, $\beta_{\text{ic,b}}$ is a result of the evolution, depending on the initial parameters A and β_i of the pre-collapse core in an a-priori unknown way.

For this reason, for each rotation profile (specified by A) we determine the boundary between pressure-dominated and centrifugal bounce in terms of the initial rotation rate β_i and the effective adiabatic index γ_{eff} by systematic numerical simulations. For models with a simple hybrid EoS ²⁵ and no deleptonization, using the same initial density profile as in the microphysical models, the results are shown in Fig. 4, both in the Newtonian case (dashed lines) and in GR (solid lines). As is apparent, for our choice of initial rotation the influence of GR can be approximated by adding an offset of $-\Delta\gamma_{\text{gr}} \simeq 0.015$ to the Newtonian results (dotted lines). This gives a

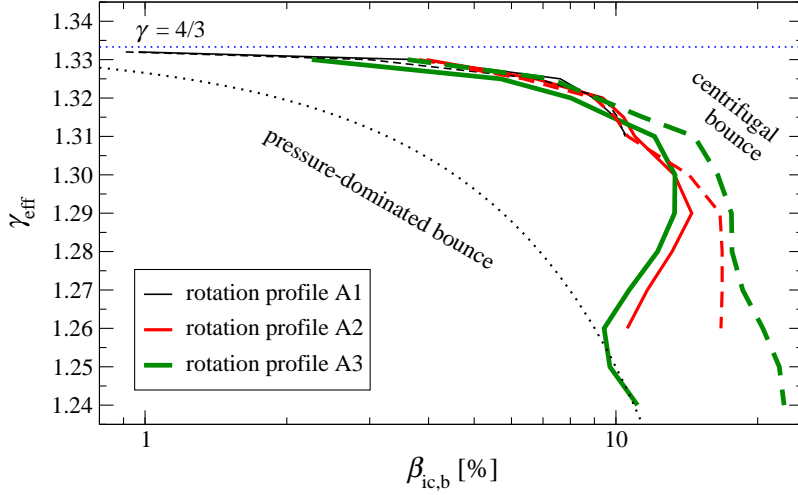


Figure 3: Boundary between pressure-dominated and centrifugal bounce in the $\gamma_{\text{eff}}-\beta_{\text{ic,b}}$ plane for models using the hybrid EoS in Newtonian gravity (dashed lines) and GR (solid lines). In a dynamical core collapse the simple Newtonian analytic relation (curved black dotted line), which additionally assumes equilibrium, strongly underestimates the correct value for $\beta_{\text{ic,b}}$ in a wide range of γ_{eff} for all investigated rotation profiles.

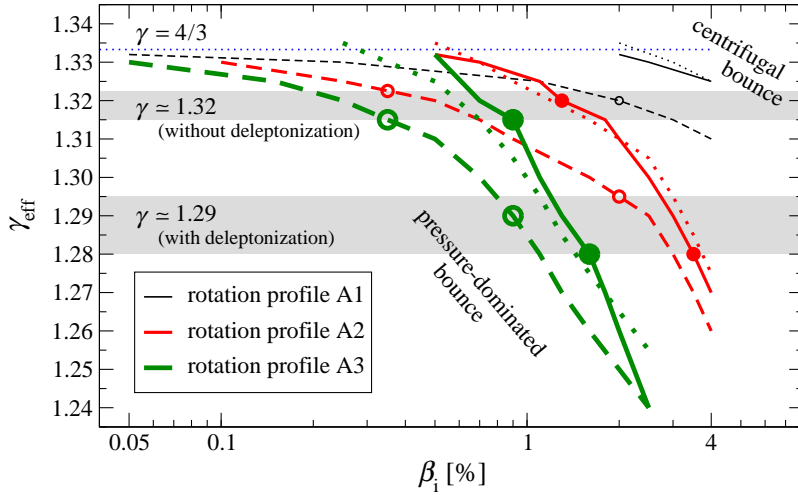


Figure 4: Boundary between pressure-dominated and centrifugal bounce in the $\gamma_{\text{eff}}-\beta_1$ plane for models using the hybrid EoS in Newtonian gravity (dashed lines) and GR (solid lines). The curved dotted lines show the Newtonian results shifted by $-\Delta\gamma_{\text{gr}} = 0.015$. The transition points for models using the microphysical EoS without and with deleptonization, again for Newtonian gravity (circles) and GR (bullets), lie in the shaded areas around $\gamma_{\text{eff}} \approx 1.32$ and 1.29 , respectively.

quantitative measure of the GR effects on rotational core collapse, which is in agreement with⁴. Note that $\Delta\gamma_{\text{gr}}$ is negative because GR effectively acts like a softening of the EoS.

For all 54 microphysical models, we find that the maximum density ρ_{max} in the core during and after bounce is always higher in GR than in Newtonian gravity, an observation that is well known from models with the simple hybrid EoS⁴. In the nonrotating limit, the difference in ρ_{max} is roughly 10%, growing strongly with increasing rotation (obviously in particular for cases where GR produces a regular bounce while Newtonian gravity results in a centrifugal bounce). As a consequence, the density crossing phenomenon discussed in detail for models with a hybrid EoS in⁴ also occurs if microphysics is taken into account (see left panel of Fig. 5). In the central parts of the PNS, the effectively stronger gravitational pull of GR results in a higher density, while the core exhibits a lower density compared to a Newtonian simulation outside a density crossing radius r_{cr} . Thus the PNS is more compact in GR.

However, in contrast to previous simulations using the hybrid EoS, for the microphysical models we do not find a clear indication that the influence of GR consistently leads to higher infall velocities v_r in the contraction phase and higher rotation velocities v_φ during and after core bounce. While our simulations confirm the results using the simpler models in⁴ that the higher compactness of the PNS in GR translates to a smaller radius for the maximum of v_φ , as shown in Fig. 5, the differences in the maximum values for both v_r and v_φ are too small to be significant. This already indicates that the effect of the GR correction $-\Delta\gamma_{\text{gr}} \approx 0.015$ is smaller

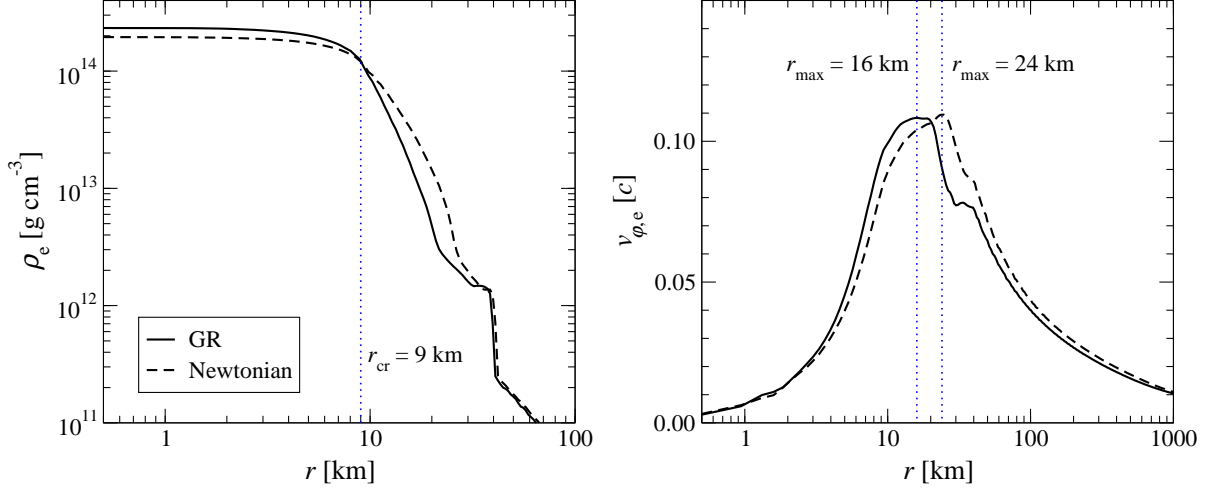


Figure 5: Left panel: Radial profile of the density ρ_e in the equatorial plane shortly after core bounce for the microphysical model with rotation profile A1 and initial rotation rate $\beta_i = 1.10\%$ in Newtonian gravity (dashed line) and GR (solid line). In the central region at radii smaller than the density crossing radius $r_{\text{cr}} = 9$ km the density is higher in GR. Right panel: Radial profiles of the rotation velocity $v_{\varphi,e}$ in the equatorial plane shortly after core bounce for the same model. The vertical lines indicate the radius r_{max} of the rotation velocity maximum.

than the influence due to microphysics, which we investigate in the following.

3.3 Influence of the Microphysical Equation of State

Fig. 4 also shows for each rotation profile the locations where the transition between pressure-supported and centrifugal bounce occurs when the microphysical EoS is used and β_i is gradually increased from 0.05% to 4%. These transitions are marked on the different boundary lines and allow the identification of the γ_{eff} value where models with the hybrid EoS make this transition. For simulations with microphysical EoS but no deleptonization we find that in all cases the transition occurs near $\gamma_{\text{eff}} \simeq 1.32$ (highlighted by the upper grey band in Fig. 4). This value agrees with the average of γ_{eos} for the microphysical EoS at densities between 10^{12} and 10^{14} g cm^{-3} (see right panel of Fig. 2), which is the most relevant range for the collapse dynamics. Thus the type of core bounce obtained with the microphysical EoS is well reproduced by the simple hybrid EoS (which is identical to a polytrope before core bounce) with $\gamma_{\text{eos}} \simeq 1.32$.

3.4 Influence of Deleptonization and Suppression of Type II Collapse

Deleptonization before neutrino trapping reduces γ_{eff} compared to γ_{eos} locally according to $\Delta\gamma_e = \frac{4}{3} \delta \ln Y_e / \delta \ln \rho|_m < 0$ (along trajectories of a collapsing fluid element m ; see^{26,2}), resulting in an effective softening of the EoS. Above trapping density at ρ_{trap} an additional positive correction $\Delta\gamma_\nu \approx \delta(P_\nu/P) / \delta \ln \rho|_m$ (assuming that $P_\nu \ll P$) due to neutrino radiation pressure effects must be considered. From the Y_e - ρ trajectories used to describe the deleptonization during core collapse, $\Delta\gamma_e$ amounts to about -0.06 to -0.05 , while a simple analytic estimate for $\Delta\gamma_\nu$ yields roughly 0.03. We thus anticipate values between -0.03 and -0.02 for the sum $\Delta\gamma_e + \Delta\gamma_\nu$, again in the density regime relevant for the bounce dynamics. Adding this correction to $\gamma_{\text{eos}} \simeq 1.32$ we expect an effective adiabatic index $\gamma_{\text{eff}} \approx 1.29$ for models with microphysical EoS and deleptonization. Again this cumulative value agrees with the results obtained in our simulations. Fig. 4 shows that the bullets and circles marking those models on the different boundary lines (for the investigated initial rotation profiles with either Newtonian gravity or GR) all lie in the range of values indicated by the lower grey band around $\gamma_{\text{eff}} \simeq 1.29$.

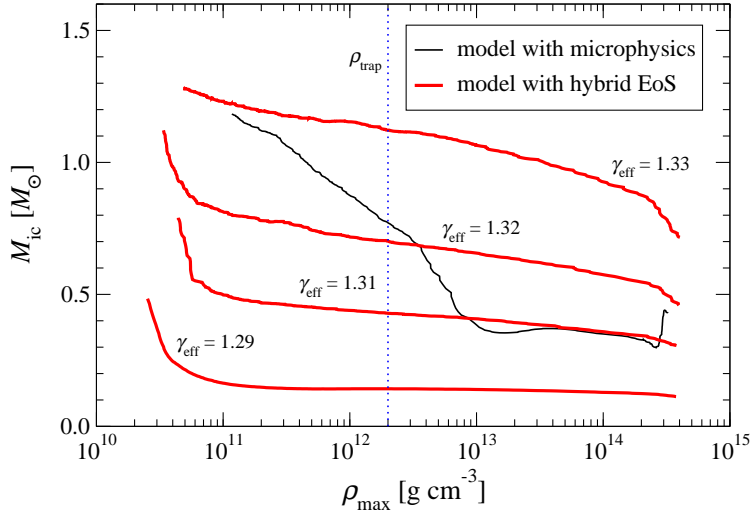


Figure 6: Mass M_{ic} of the homologically collapsing inner core in the entire density range of the maximum density ρ_{max} in the core during a nonrotating collapse in GR. The value of M_{ic} at the high density end point of the curves corresponds to the mass $M_{ic,b}$ of the inner core at bounce. While the value of M_{ic} for models with a simple hybrid EoS is already approximately determined at low densities (red curves), in the microphysical model it decreases considerably around neutrino trapping density ρ_{trap} (black curve), albeit only to a value that is significantly higher than if the hybrid EoS with $\gamma_{eff} = 1.29$ is used.

The finding that deleptonization decreases γ_{eff} to about 1.29 explains the absence of Type II GW signals for all our models in GR with microphysics. When a hybrid EoS is used, the subgroup of such models showing multiple centrifugal bounces and subsequent strong re-expansion phases of the inner core occupies only a small area in the $\gamma_{eff}-\beta_i$ plane. It is located at $\gamma_{eff} \geq 1.31$ for all of our initial rotation states both in the Newtonian case and in GR, i.e. significantly above the value of $\gamma_{eff} \simeq 1.29$ that characterizes the microphysical models if deleptonization is included.

3.5 Mass of the Inner Core at the Time of Bounce and Suppression of Type III Collapse

The value $\gamma_{eff} = 1.29$ captures well the deleptonization effects in the density regime between 10^{12} and 10^{14} g cm^{-3} (i.e. above neutrino trapping). Therefore it serves as a good criterion to determine the high density collapse dynamics and also the core bounce behavior. Consequently, models with hybrid EoS and $\gamma_{eos} = 1.29$ exhibit the same collapse and bounce behavior in this dynamical phase. Nevertheless, the global assumption $\gamma_{eff} = 1.29$ fails to correctly predict the mass $M_{ic,b}$ of the inner core at bounce for the microphysical models. For this value of the effective adiabatic index, by equating the pressures of two polytropes $P = K(Y_{e,i} = 0.5) \rho^{\gamma_{eff}}$ and $P = K(Y_e) \rho^{4/3}$ with $K = K' Y_e^{4/3}$ and constant $K' = 1.2435 \times 10^{15}$ (in cgs units) for a relativistic degenerate electron gas, the hybrid EoS yields an effective average Y_e of ≈ 0.237 assuming a typical mean density in the core of $\rho = 10^{10}$ g cm^{-3} during collapse. Using this estimate for models with the hybrid EoS we find a small mass $M_{ic} \sim 0.1 - 0.3 M_\odot$ (higher for more rapid rotation), consistent with the theory of self-similar collapse²⁷. Due to the instantaneous initial pressure reduction throughout the entire core in the case of the hybrid EoS, the final value $M_{ic,b}$ at the time of bounce is already determined at low densities (see Fig. 6, where we plot the change of M_{ic} with the maximum density ρ_{max} in the core during collapse for models without rotation).

In models with microphysics however, in the early collapse phase at low densities the effective adiabatic index γ_{eff} is significantly higher than 1.29, both because the adiabatic index γ_{eos} of the EoS is much closer to $4/3$ (see Fig. 2) and because deleptonization is weak at those densities. This results in a high initial value $M_{ic} \simeq 1.2 M_\odot$ for the mass of the inner core (see Fig. 6). At intermediate densities *around* the neutrino trapping density ρ_{trap} , deleptonization indeed reduces M_{ic} , but only to about $0.5 - 0.9 M_\odot$ (increasing with rotation). In the late, high density phase of the collapse, M_{ic} then stays roughly constant until core bounce. This behavior is in agreement with recent spherically symmetric GR results using Boltzmann neutrino transport²⁸.

Therefore, even by taking into account the *local* influence of deleptonization the microphysical models end up with a significantly larger mass $M_{ic,b}$ of the inner core at bounce than the

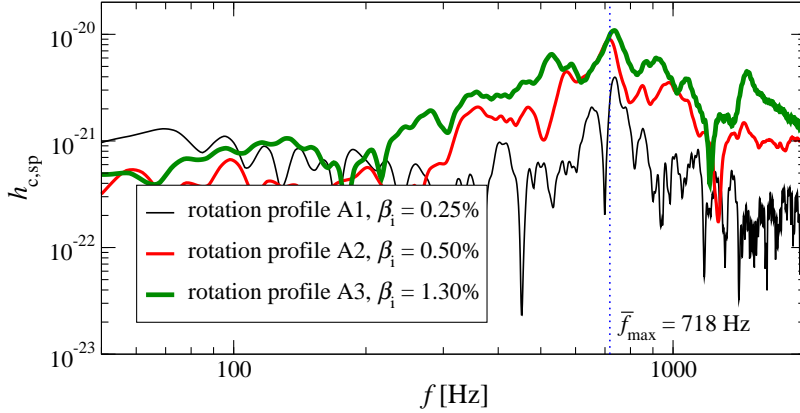


Figure 7: Characteristic GW strain spectra $h_{c,sp}$ at a distance $d = 10$ kpc to the source for three representative models in GR with microphysical EoS and deleptonization that do not undergo centrifugal bounce. As for most other models the individual maxima f_{\max} of their frequency spectrum is very close to $\bar{f}_{\max} \simeq 718$ Hz.

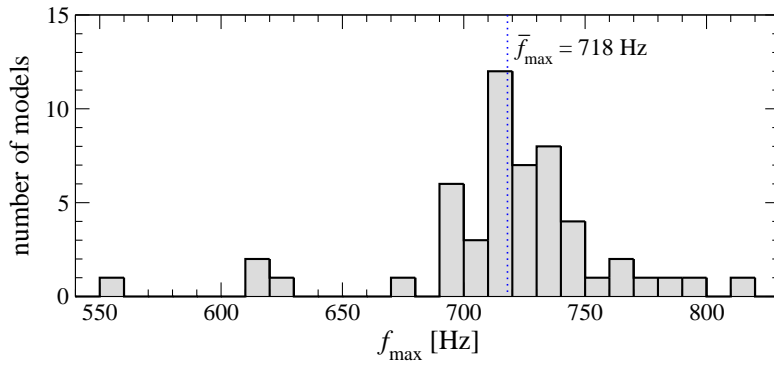


Figure 8: Histogram of the maxima f_{\max} of the waveform's frequency spectrum for all 54 GR models with microphysical EoS and deleptonization. The values of f_{\max} for most models are spread in a very narrow frequency range around the average value located at $\bar{f}_{\max} \simeq 718$ Hz.

models with a simple hybrid EoS with γ_{eff} which undergo a *global* initial reduction of pressure. This explains the complete absence of rapid collapse dynamics and the according Type III GW burst signals in our models, which only occurs for $M_{\text{ic}} \lesssim 0.2 M_{\odot}$ (see also the discussion in ⁵).

3.6 Detectability of the Gravitational Wave Signal

The generic nature of the GW burst signal has several important implications for prospective detectability. The limitation to a unique Type I waveform for a very broad range of rotation states of the progenitor core will very likely facilitate the use of more powerful and finetuned data analysis methods in GW detectors. To this end, we offer our results in a publicly accessible waveform catalog ^a. Note that almost all investigated models result in a pressure-dominated bounce and instantaneous formation of a PNS with similar average density and compactness. For these models, whose rotation rates at bounce span two orders of magnitude ($0.2\% \lesssim \beta_{\text{ic,b}} \lesssim 20\%$), the individual maxima f_{\max} of their waveform's frequency spectrum lie for most models in a very narrow range with an average of $\bar{f}_{\max} \simeq 718$ Hz. This is exemplified in Fig. 7, where the characteristic GW strain spectrum $h_{\text{char}} = d^{-1} \sqrt{2\pi^{-2} dE_{\text{GW}}/df}$ (with E_{gw} being the energy emitted in GWs and $d = 10$ kpc being the distance to the source) ^{29,15} for three representative models that do not undergo centrifugal bounce is plotted.

The clustering in frequency can also be clearly seen in the histogram in Fig. 8, where all 54 GR models with microphysical EoS and deleptonization are shown. This property of the GW burst signal could potentially become important for a possible detectability by detectors of both interferometric and resonant type. In Fig. 9 we plot the (detector-dependent) frequency-integrated characteristic waveform amplitude h_c against the characteristic frequency f_c (Eq. (31) in ³⁰) for all 54 GR models with microphysical EoS and deleptonization. We assume optimal orientation of source and detector, and in cases with pressure-dominated bounce remove the

^awww.mpa-garching.mpg.de/rel_hydro/wave_catalog.shtml.

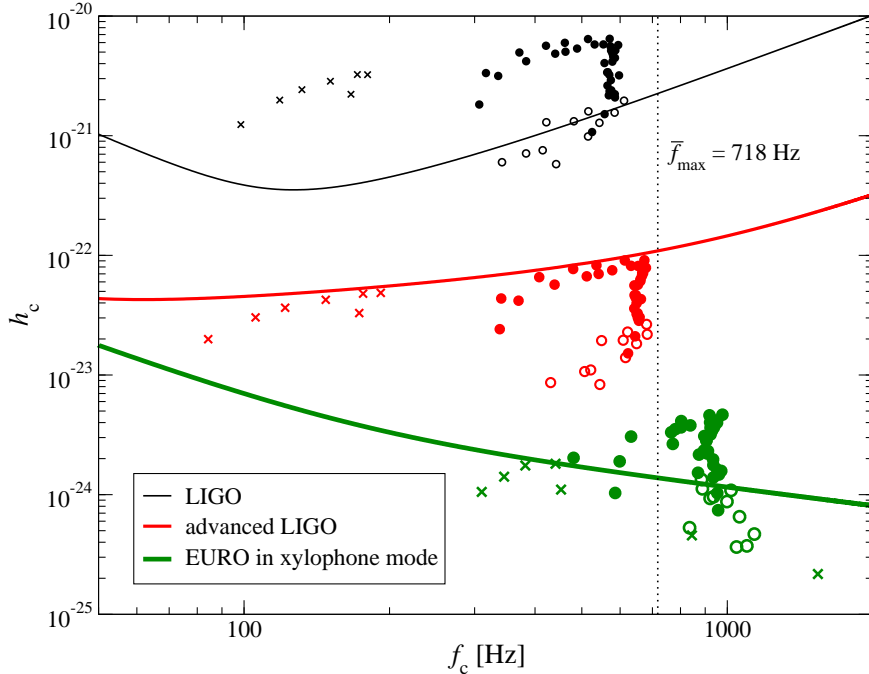


Figure 9: Location of the GW burst signals from the core bounce for all models in the h_c - f_c plane relative to the sensitivity curves of various GW interferometer detectors (as color-coded). The sources are at a distance of 10 kpc for LIGO, 0.8 Mpc for advanced LIGO, and 15 Mpc for EURO. Open circles denote models where the filtered-out early postbounce convection contributes significantly to the original signal, and crosses show models undergoing centrifugal bounce.

lower-frequency contribution from the post-bounce convective overturn by cutting the spectrum below 250 Hz, as we are only interested in the GW signal from the bounce and ring-down. Fig. 9 shows that while current LIGO class interferometric detectors are only sensitive to signals coming from an event in the Milky Way, advanced LIGO could marginally detect some signals from other galaxies in the Local Group like Andromeda. For the proposed EURO detector^b in xylophone mode, we expect a very high signal-to-noise ratio (which is h_c divided by the detector sensitivity at f_c). This detector could also measure many of the computed signals at a distance of 15 Mpc, i.e. in the Virgo cluster.

Note that detectability could be enhanced by (i) a network of interferometers in coincidence search, (ii) the support by resonant detectors, which is particularly facilitated by the narrow range of f_{\max} , and (iii) the use of more powerful data analysis methods beyond time-frequency analysis (see³¹ and references therein) based on the waveforms' similarity and robustness. A serious obstacle for detection is the low event rate of $\sim 1 \text{ yr}^{-1}$ within 15 Mpc (or at most $\sim 5 \text{ yr}^{-1}$ including the entire Virgo cluster^{32,33,34}), which is further reduced by assuming that only a small fraction (possibly only 1%) of all progenitors rotate fast enough to have a strong GW bounce signal³⁵. Nevertheless, our results can serve as a guideline for a possible frequency narrow-banding of future interferometers (which can significantly boost sensitivity), as well as for choosing the optimal configuration in the planning of resonant detectors like the proposed DUAL detector³⁶. In addition, as a core collapse may be accompanied by other GW emission mechanisms of comparable strength like late-time convection (also in a nonrotating core), PNS pulsations, or bar-mode instabilities, the *total* GW signal strength and duration could be significantly higher than predicted here.

As a downside, the generic properties of the GW burst signal introduce a frequency degeneracy into the signal inversion problem. Consequently, in the case of a detection it is difficult to extract details about the rotation state of the pre-collapse core, because a large part of the corresponding parameter space yields a pressure-dominated bounce and thus signals with very similar values for f_{\max} and (depending on the detector) also for f_c . On the other hand, as f_{\max} directly depends on the compressibility of the nuclear EoS at bounce, determining this frequency

^bwww.astro.cardiff.ac.uk/geo/euro/.

from the GW burst signal can help to constrain the EoS properties around nuclear density.

Acknowledgments

We thank D. Shoemaker for helpful discussions. This work was supported by DFG (SFB/TR 7 and SFB 375). H.D. is a Marie Curie Intra-European Fellow within the 6th European Community Framework Programme (IEF 040464), and C.D.O. acknowledges support by the Joint Institute for Nuclear Astrophysics (JINA) under NSF grant PHY0216783.

References

1. E. Müller, *Astron. Astrophys.* **114**, 53 (1982).
2. R. Mönchmeyer *et al*, *Astron. Astrophys.* **246**, 417 (1991).
3. T. Zwerger and E. Müller, *Astron. Astrophys.* **320**, 209 (1997).
4. H. Dimmelmeier, J. Font, and E. Müller, *Astron. Astrophys.* **393**, 523 (2002).
5. K. Kotake, S. Yamada, and K. Sato, *Phys. Rev. D* **68**, 044023 (2003).
6. C. D. Ott *et al*, *Astrophys. J.* **600**, 834 (2004).
7. C. D. Ott *et al*, *Phys. Rev. Lett.*, accepted (2007).
8. H. Dimmelmeier *et al*, *Phys. Rev. Lett.*, accepted (2007).
9. M. Rampp, E. Müller, and M. Ruffert, *Astron. Astrophys.* **332**, 969 (1998).
10. E. Müller *et al*, *Astrophys. J.* **603**, 221 (2004).
11. M. Shibata and Y.-I. Sekiguchi, *Phys. Rev. D* **71**, 024014 (2005).
12. C. D. Ott *et al*, *Phys. Rev. Lett.* **96**, 201102 (2006).
13. C. D. Ott *et al*, *Class. Quantum Grav.*, accepted (2007).
14. L. Blanchet, *Living Rev. Relativity*, **9**, 4 (2006), URL (cited on 15.05.2007): <http://www.livingreviews.org/lrr-2006-4>.
15. H. Dimmelmeier *et al*, *Phys. Rev. D* **71**, 064023 (2005).
16. J. A. Isenberg, University of Maryland Preprint (1978), gr-qc/0702113
17. J. R. Wilson, G. J. Mathews, and P. Marronetti, *Phys. Rev. D* **54**, 1317 (1996).
18. M. Shibata and Y.-I. Sekiguchi, *Phys. Rev. D* **69**, 084024 (2004).
19. H. Shen *et al*, *Prog. Theor. Phys.* **100**, 1013 (1998).
20. A. Marek *et al*, *Astron. Astrophys.* **443**, 201 (2005).
21. M. Liebendörfer, *Astrophys. J.* **633**, 1042 (2005).
22. K. Langanke and G. Martínez-Pinedo, *Nucl. Phys. A* **673**, 481 (2000).
23. S. E. Woosley, A. Heger, and T. A. Weaver, *Rev. Mod. Phys.* **74**, 1015 (2002).
24. J. E. Tohline, *Astrophys. J.* **285**, 721 (1984).
25. H.-T. Janka, T. Zwerger, and R. Mönchmeyer, *Astron. Astrophys.* **268**, 360 (1993).
26. K. A. van Riper and J. M. Lattimer, *Astrophys. J.* **249**, 270 (1981).
27. A. Yahil, *Astrophys. J.* **265**, 1047 (1983).
28. W. R. Hix *et al*, *Phys. Rev. Lett.* **91**, 201102 (2003).
29. É É Flanagan and S. A. Hughes, *Phys. Rev. D* **57**, 4535 (1998).
30. K. S. Thorne, in *300 Years of Gravitation*, ed. S. W. Hawking and W. Israel (Cambridge University Press, Cambridge, UK, 1987).
31. N. Arnaud *et al*, *Phys. Rev. D* **67**, 062004 (2003).
32. N. Arnaud *et al*, *Astropart. Phys.* **21**, 201 (2004).
33. P. Nutzman *et al*, *Astrophys. J.* **612**, 364 (2004).
34. R. G. Izzard, E. Ramirez-Ruiz, and C. A. Tout, *Mon. Not. R. Astron. Soc.* **348**, 1215 (2004).
35. S. E. Woosley and A. Heger, *Astrophys. J.* **637**, 914 (2006).
36. M. Cerdonio *et al*, *Phys. Rev. Lett.* **87**, 031101 (2001).